Chapter 6

Bistability and stochastic phenomena

Abstract The bistability of the reaction observed on Sample C depends on the intensive parameters x_{CO} and T. Hence, no size effects should be expected, which would explain the quenching of the bistability on Sample A and Sample B. However, Sample A and Sample B differ in two ways from Sample C: First, the proportion of defect sites over regular sites is larger on smaller samples. These sites have different electronic properties and can therefore have a large influence on the reaction rate. Second, the discrete principle of a reaction implies the existence of stochastic fluctuations. The intensity of fluctuations varies with $N^{-1/2}$, where N is the size of the system. Fluctuations can therefore be rapidly neglected as the system grows (i.e. on Sample C), where they can have a large importance on smaller systems (i.e. Sample A and Sample B). Asynchronous fluctuations on an ensemble of particles would lead to an average steady state. These two phenomena can therefore explain that the bistability was not measured on smaller samples and are investigated in this chapter by means of experiments and simulations.

6.1 Global reaction rates under transient conditions

On Figure 6.1, we apply the approach used in Section 5.3 to the three different samples. That is, the surface is exposed to one beam, then, the complementary gas is introduced. x_{CO} is chosen where the transition from O-rich to CO-rich occurs and where hysteresis is expected.

Sample A Figure 6.1a shows that a common steady state is reached, independently of the experimental conditions. The timescale at which the steady state is established is typically within experimental accuracy.

Sample B On Figure 6.1b, the reaction rate established just after admission of the complementary beam is different when starting from a CO-precovered or an O-precovered surface. However, the differences vanish slowly but completely on a typical timescale of 100 s. Note that this behavior occurs on a large range of xco and for different temperatures, and not only for the conditions pictured Figure 6.1b.

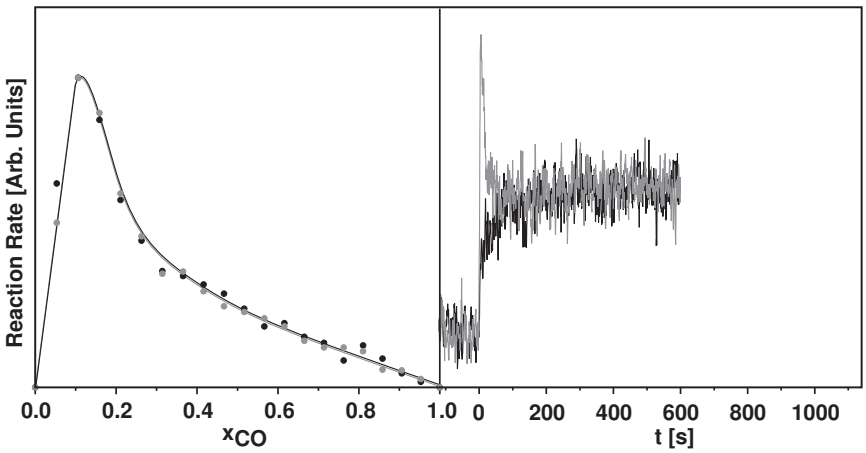

(a) Sample A; Left: steady-state rate after 180 s, $T = 400$ K; Right: transient at $x_{\mathrm{CO}} = 0.26$, $T = 415$ K

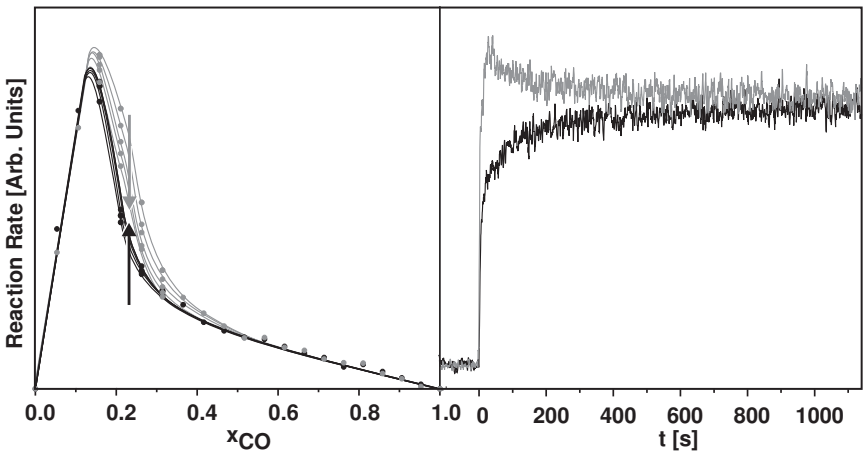

(b) Sample B; Left: steady-state rate after 180, 300, 420, 600 and 800 s, $T = 400$ K; Right: transient at $x_{\mathrm{CO}} = 0.26$, $T = 415$ K

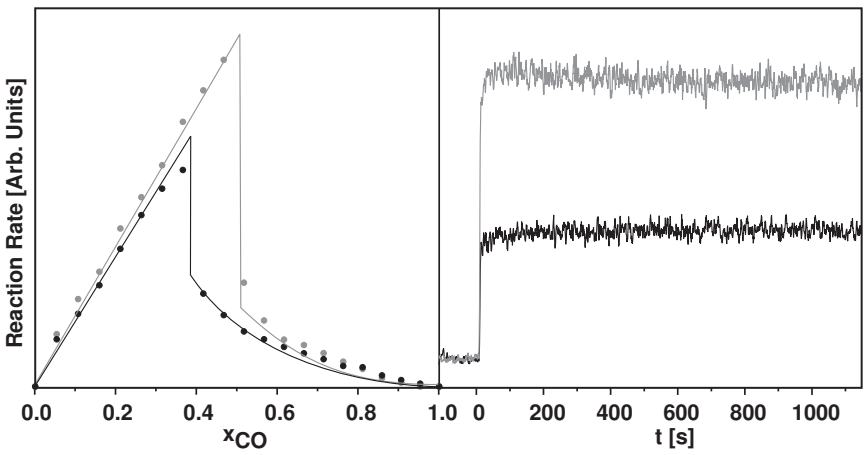

(c) Sample C; Left: steady-state rate after 180 s, $T = 400$ K; Right: transient at $x_{\mathrm{CO}} = 0.52$, $T = 415$ K

Figure 6.1. CO_2 production rates at steady state as a function of xco (left) and during the transient as a function of time (right); black: CO-precovered, gray: O-precovered. The bistability vanishes with smaller particle size.

Sample C Figure 6.1c shows a typical transient observed within the bistable region (also see Section 5.3). A different steady state is established for experiments on a CO- or O-precovered surface. The transients show that this state is perfectly stable on a timescale above 1000 s.

The bistability is therefore observable on particles down to 500 nm size. However, it vanishes completely for smaller particles. The transition to monostable global kinetics proceeds in a continuous fashion: The lifetime of the global reactive states decreases with decreasing particle size. As afore mentioned, there are two possible effects which may lead to a vanishing bistability in the small particle limit:

- The presence of defect sites such as edges, steps, corners or interface sites increases with decreasing particle size. As a result of the differences in chemisorption energy at such sites, their presence should result in an increased coverage dependence of the adsorption energies. Indeed, such an effect has been verified experimentally for CO adsorption and oxidation on the model catalyst utilized in this work [73, 102]. With respect to the bistable behavior, Zhdanov and Kasemo has shown that an increasing coverage dependence of the CO_{ad} desorption energy leads to a decreasing extension of the bistability region [9]. However, up to now there are no experimental verifications of such an effect. The high defect density on small particles is likely to generate a coverage dependence of CO adsorption energy, which in turn may potentially lead to a quenching of the kinetic bistability.

- The influence of coverage fluctuations is also size dependent. In the limit of negligible surface diffusion via the oxide support, which interacts only weakly with the reactants [103], the particles act like isolated nanoreactors. On their confined surface area, the amplitude of coverage fluctuations increases with decreasing particle size. Therefore, an increasing probability for fluctuation-induced transitions between the two kinetic regimes is expected as the particles become smaller. Similar fluctuation-related confinement effects are expected in cases of limited adsorbate mobility [64]. Experimentally, fluctuation-induced transitions have indeed been observed for CO oxidation on a Pt field emitter tip, exhibiting facets in the size range of a few nanometers and the results could be theoretically reproduced by means of hybrid Monte Carlo (MC)–MF simulations [104–107]. In the case of a macroscopic catalyst sample, fluctuation-induced kinetic transitions should eventually result in the formation of a dynamic equilibrium between both reactive states and, consequently, in macroscopically monostable kinetics. Indeed, disappearance of bistability and hysteresis effects on facets exposing significantly less than 10^2 adsorption sites, was recently predicted, based on MC simulations [108]. Thus we might speculate that the rarity of reported bistability effects on supported catalysts and model catalysts may be due to the role of such fluctuation-induced transitions.

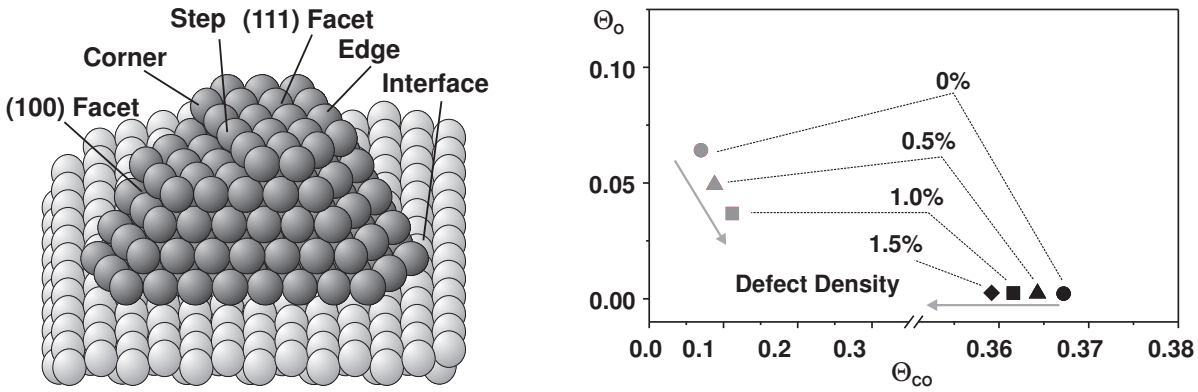

(a) (b) HeMF; $x_{CO} = 0.48$, $T = 415\,\mathrm{K}$

Figure 6.2. (a) atomic representation of Sample B showing the "perfect" (111) facets and the "defect"-rich (100) facets; (b) steady-state coverages for increasing defect density as calculated with HeMF.

6.2 Establishment of the heterogeneous mean field model

6.2.1 Heterogeneous surface

To determine the importance of either effect is extremely difficult experimentally. We therefore rely on simulations. Firstly, an heterogeneous mean field model (HeMF) is established based on HoMF (see Section 3.2). The defect sites are represented by a fraction of the surface with a lower binding energy for CO_{ad} and a lower reaction barrier. The new energies chosen remain consistent with the literature [46, 64, 86, 102]. Moreover, coupling between the different sites is allowed due to the MF foundations of the model. The approach taken here differs only slightly from Ref. [86] in that oxygen is now allowed to diffuse freely between the different sites. This is a requirement of the integration of the coupled MF ODEs Eq. 3.4. We therefore refer the reader to Ref. [86] for the complete argumentation based on thermodynamical arguments.

Two separate integrations of HoMF are performed, one with the energies of the so-called perfect sites and one with the energies of the defect sites. Then the coverages are shared according to

$$\frac{\Theta_{CO}^{Perfect,max} - \Theta_{CO}^{Perfect}}{\Theta_{CO}^{Perfect}} \frac{\Theta_{CO}^{Defect}}{\Theta_{CO}^{Defect,max} - \Theta_{CO}^{Defect}} = \exp\left(\frac{E_{des}^{Defect} - E_{des}^{Perfect}}{RT}\right), \tag{6.1a}$$

$$\Theta_{CO}^{tot} = \chi\Theta_{CO}^{Defect} - (1-\chi)\Theta_{CO}^{Perfect}, \tag{6.1b}$$

$$\Theta_{O}^{tot} = \chi\Theta_{O}^{Defect} - (1-\chi)\Theta_{O}^{Perfect}. \tag{6.1c}$$

for a fraction χ of defect sites. No differences between the binding energies of O_{ad} on the defect or perfect sites are considered due to the absence of relevant literature data. O_{ad} is thus distributed proportionally in Eq. 6.1c, which is certainly not realistic.

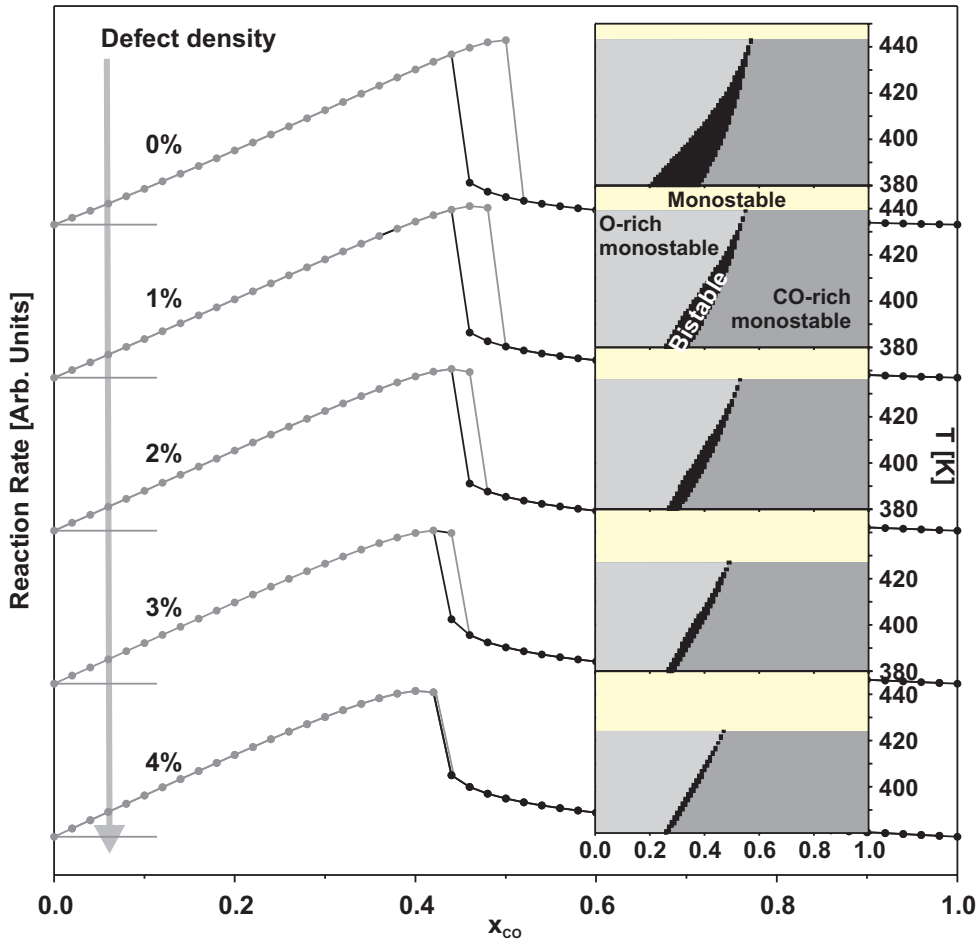

Figure 6.3. HeMF for defect densities $0 \leqslant \chi \leqslant 0.04$. The steady-state rates as a function of x_{CO} are calculated at $T = 415$ K and phase diagram (inset) as a function of x_{CO} and T. Increasing defect density reduces the size of the bistable phase.

6.2.2 Validation of the model

The parameters for this model are those of HoMF (Table 3.2). The activation energies for defect sites are chosen below the fitted values of perfect sites and remain in agreement with the literature [46, 64, 89]. Values of $E'^{\mathrm{des}}_{\mathrm{CO}} = 117\,\mathrm{kJ\,mol^{-1}}$ and $E'_{\mathrm{LH}} = 44\,\mathrm{kJ\,mol^{-1}}$ are assumed to be reasonable and are used in HeMF. Further validation of the model is not necessary as the results are those of HoMF for $\chi = 0$.

6.3 Simulations with the heterogeneous mean field model

Figures 6.2 and 6.3 show systematic simulations of the kinetics as a function of the fraction of weakly adsorbing $\mathrm{CO_{ad}}$ sites. As expected on the basis of previous work [9], we find that the width of the bistable region rapidly decreases with increasing defect density.

However, in spite of the pronounced influence of surface defects on the nature of the bistability region, a thorough inspection of the transient behavior shows that there are no indications for a fundamentally modified transient behavior. In particular, the appearance of unusually slow transient kinetics, as observed experimentally with Sample B, cannot be explained by the influence of defects. We thus conclude that the particle-size dependent bistability effect cannot be attributed to the presence of defects alone.

6.4 Establishment of the stochastic model

6.4.1 Establishment of the master equation

Fluctuations come from the discrete nature of chemical reactions (see, e.g., Ref. [20]). MF treatments, which describe the reaction with continuous values (i.e. coverages), are intrinsically deterministic. However, the MF models used allow a suitable description of the reaction in the large-size limit. It is therefore important to retain the informations from these models. The approach is therefore to define the rate per site $W_j(\mathbf{N})$ (unit $s^{-1}cm^{-2}$) for each step j of the reaction mechanism as a function of the population $\mathbf{N}$ at the surface of the catalyst and of $w_j(\mathbf{\Theta})$ as defined in the MF models. This is achieved by the simple relation

$$W_j(\mathbf{N}) = w_j(\mathbf{\Theta})\, N_{\mathrm{Pd}}. \tag{6.2}$$

A comparison with the definition of the coverages Eq. 3.1 shows that Eq. 6.2 corresponds to a change of scale.

Each time one elementary reaction is performed, a net change of the population $\mathbf{M_j}$ as defined in Table 6.1 occurs. $W_j(\mathbf{N})$ is the rate at which these events happen. Now, the probability of finding the system in the state $(\mathbf{N} - \mathbf{M_j}, t + \Delta t)$ at time $t + \Delta t$, is given by the sum of the rate of all the processes that can occur at $(\mathbf{N}, t)$ multiplied by the probability for them to occur

$$P(\mathbf{N} - \mathbf{M_j}, t + \Delta t) = \sum_{j=1}^{4} \left[P(\mathbf{N}, t)\, W_j(\mathbf{N})\right], \qquad \text{Chapman-Kolmogorov equation.}$$

The new population $(\mathbf{N} - \mathbf{M_j})$ again obeys the same probability laws for the next Δt (i.e. it is a Markov process). In other words, the time evolution of the system is fully

Process	Population change	Net change $\mathbf{M}$	Rate $s^{-1}cm^{-2}$
CO adsorption	$(N_{\mathrm{CO}}, N_{\mathrm{O}}) \rightarrow (N_{\mathrm{CO}} + 1, N_{\mathrm{O}})$	$(+1, 0)$	$W^{\mathrm{ad}}_{\mathrm{CO}}$
CO desorption	$(N_{\mathrm{CO}}, N_{\mathrm{O}}) \rightarrow (N_{\mathrm{CO}} - 1, N_{\mathrm{O}})$	$(-1, 0)$	$W^{\mathrm{des}}_{\mathrm{CO}}$
O_2 adsorption	$(N_{\mathrm{CO}}, N_{\mathrm{O}}) \rightarrow (N_{\mathrm{CO}}, N_{\mathrm{O}} + 2)$	$(0, +2)$	$W^{\mathrm{ad}}_{\mathrm{O_2}}$
Reaction	$(N_{\mathrm{CO}}, N_{\mathrm{O}}) \rightarrow (N_{\mathrm{CO}} - 1, N_{\mathrm{O}} - 1)$	$(-1, -1)$	W_{LH}

Table 6.1. The four elementary processes of the Langmuir-Hinshelwood mechanism expressed as probability laws.

determined by the initial distribution, or, for $\Delta t \to 0$,

$$\frac{dP(\mathbf{N}-\mathbf{M_j}, t+\Delta t) - dP(\mathbf{N}, t)}{\Delta t} = \frac{\partial P(\mathbf{N}, t)}{\partial t} = \sum_{j=1}^{4} \left[W_j(\mathbf{N}-\mathbf{M_j}) P(\mathbf{N}-\mathbf{M_j}) - W_j(\mathbf{N}) P(\mathbf{N}) \right], \quad (6.3)$$

which is the master equation (ME) [18, 19, 109]. Integration of this ODE constitutes the basis of the stochastic model (SM).

Recent publications [105, 107, 110, 111] utilize this approach to describe the oscillatory behavior of CO oxidation on Pt field electron microscopy (FEM) tips. It is noteworthy that the ME reproduces the MF equations in the limit of large scales. A second point is that, although deriving from a MF approximation, the ME is an exact method [20]. Finally, usage of MF rates implies that heterogeneous surface can simply be implemented in SM as $W_j(\mathbf{N}) \equiv \chi W_j^{\text{Defect}}(\mathbf{N}) + (1-\chi) W_j^{\text{Perfect}}(\mathbf{N})$.

6.4.2 Establishment of the stochastic model

The ME for the case of CO oxidation on Pd is

$$\begin{aligned}\frac{dP(N_{\text{CO}}, N_{\text{O}})}{dt} &= W_{\text{CO}}^{\text{ad}}(N_{\text{CO}}-1, N_{\text{O}}) P(N_{\text{CO}}-1, N_{\text{O}}) - W_{\text{CO}}^{\text{ad}}(N_{\text{CO}}, N_{\text{O}}) P(N_{\text{CO}}, N_{\text{O}}) \\ &+ W_{\text{CO}}^{\text{des}}(N_{\text{CO}}+1, N_{\text{O}}) P(N_{\text{CO}}+1, N_{\text{O}}) - W_{\text{CO}}^{\text{des}}(N_{\text{CO}}, N_{\text{O}}) P(N_{\text{CO}}, N_{\text{O}}) \\ &+ W_{\text{O}_2}^{\text{ad}}(N_{\text{CO}}, N_{\text{O}}-2) P(N_{\text{CO}}, N_{\text{O}}-2) - W_{\text{O}_2}^{\text{ad}}(N_{\text{CO}}, N_{\text{O}}) P(N_{\text{CO}}, N_{\text{O}}) \\ &+ W_{\text{LH}}(N_{\text{CO}}+1, N_{\text{O}}+1) P(N_{\text{CO}}+1, N_{\text{O}}+1) - W_{\text{LH}}(N_{\text{CO}}, N_{\text{O}}) P(N_{\text{CO}}, N_{\text{O}}).\end{aligned}$$

This ME does not have analytical solutions. In this work, we solve it numerically by means of three different algorithms:

- Euler forward method [112] for the time evolution of the system in population space;
- the algorithm proposed by Dickman [113] for fast convergence to steady state;
- MC to follow the time evolution of the population on a single particle, with a variable time step Δt such as $\Delta t \propto \sum_{j=1}^{4} W_j$ is the time a state remains.

An estimate of $(N_{\text{CO}}^{\max}, N_{\text{O}}^{\max})$ can be calculated on the basis of experimental data and saturation coverages for Sample A and Sample B, where $(N_{\text{CO}}^{\max}, N_{\text{O}}^{\max}) = (30, 15)$ and $(N_{\text{CO}}^{\max}, N_{\text{O}}^{\max}) = (270, 135)$, respectively. Taking a realistic number of surface sites for Sample C would be too expensive. As fluctuations vanish with increasing sample size, $(N_{\text{CO}}^{\max}, N_{\text{O}}^{\max}) = (1000, 500)$ is assumed to be large enough and was used for Sample C.

The initial probabilities

$$P(N_{\text{CO}}, N_{\text{O}}) = \begin{cases} 1 & \text{if } N_{\text{CO}} = 1 \text{ and } N_{\text{O}} = 0, \text{ for the CO-precovered experiments,} \\ 1 & \text{if } N_{\text{CO}} = 0 \text{ and } N_{\text{O}} = 1, \text{ for the O-precovered experiments,} \\ 0 & \text{otherwise} \end{cases}$$

are chosen to reproduce the experiments.

The global CO_2 production rate is simply the sum of the local reaction rates.

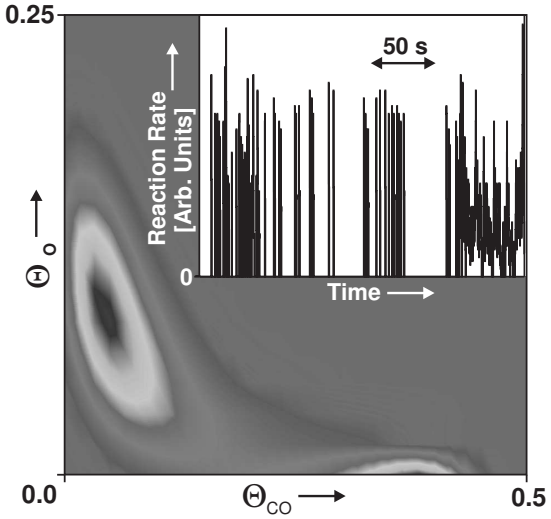

(a) Sample A, $T = 415\,\mathrm{K}$, $x_{\mathrm{CO}} = 0.46$, $\chi = 0\%$

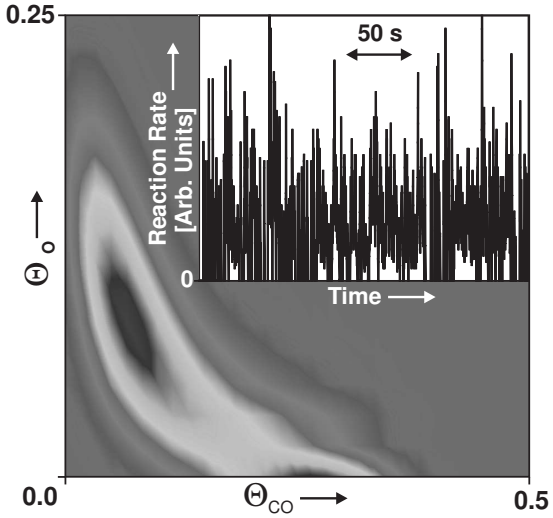

(b) Sample A, $T = 415\,\mathrm{K}$, $x_{\mathrm{CO}} = 0.50$, $\chi = 20\%$

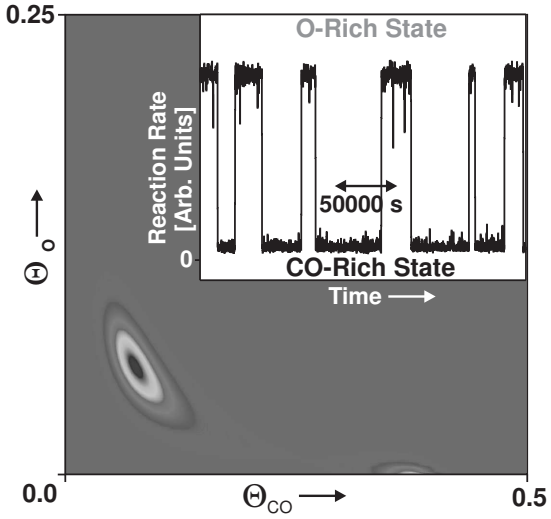

(c) Sample B, $T = 415\,\mathrm{K}$, $x_{\mathrm{CO}} = 0.49$, $\chi = 0\%$

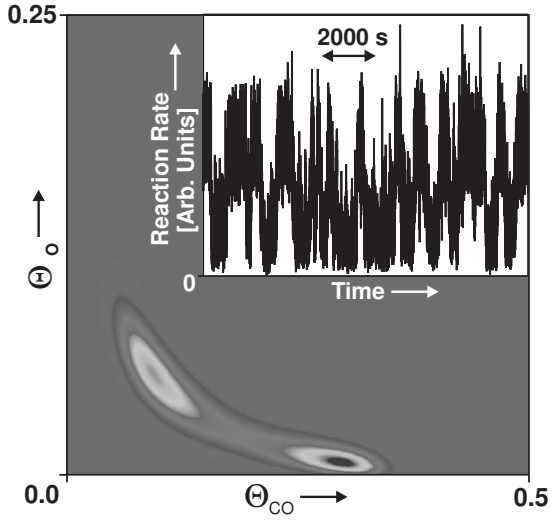

(d) Sample B, $T = 415\,\mathrm{K}$, $x_{\mathrm{CO}} = 0.52$, $\chi = 10\%$

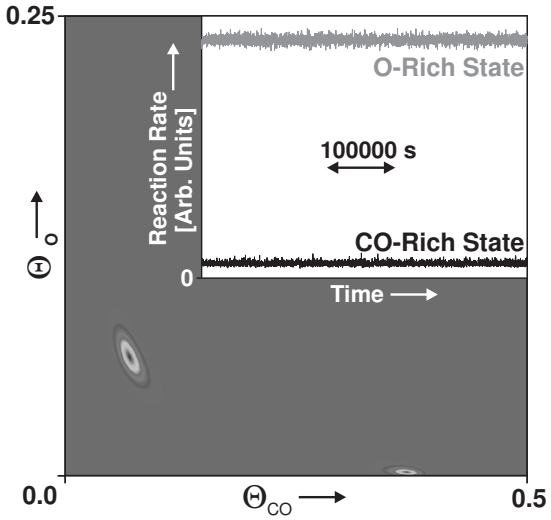

(e) Sample C, $T = 415\,\mathrm{K}$, $x_{\mathrm{CO}} = 0.48$, $\chi = 0\%$

Figure 6.4. Simulations from SM+HeMF illustrate the combined effect of limited particle size and surface defects on the kinetic bistability. Because of the increasing amplitude of fluctuations, the width of the probability distributions in coverage space increases with decreasing particle size [(a), (c) and (e)], and spontaneous transitions between both reaction regimes become more frequent. For an ensemble of particles, this results in a dynamic equilibrium being established between both reactive states. Upon modifying the reaction and adsorption probability according to HeMF, the probability maximums approach each other and the transition rates increase drastically.

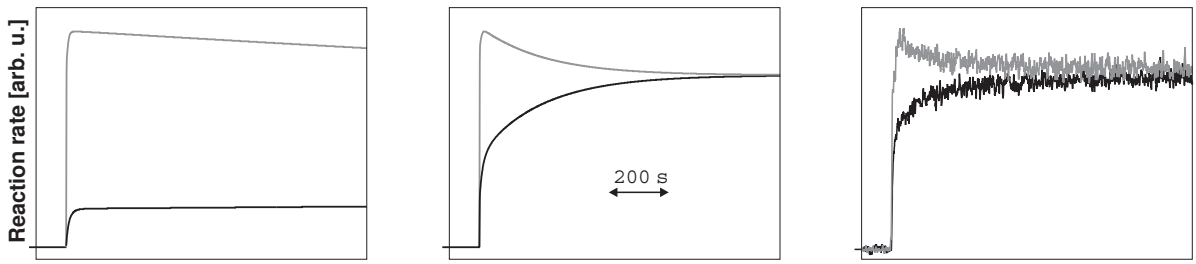

(a) SM+HeMF; Sample B, $\chi = 0\%$ (b) SM+HeMF; Sample B, $\chi = 10\%$ (c) Experiment, Sample B

Figure 6.5. Simulations using HeMF (a) and (b) need a significant defect density to fit the experiment (c) ($T = 415$ K, $x_{CO} = 0.26$).

6.5 Simulations with the stochastic model

First, the steady states are obtained from SM. Whereas the deterministic nature of the MF models represents the steady states as points in coverage space, SM gives a probability distribution (see Figure 6.4). As expected, the intensity of the fluctuations is larger for smaller systems. Indeed, the width of the probability distributions increases for decreasing particle size. For Sample A and Sample B, the probability distributions, centered on the deterministic steady states, merge. Therefore, spontaneous transitions between the steady states are allowed. However, for Sample C, the probability distribution is narrow and there are no transition probabilities. SM approaches the deterministic MF limit in the case of large surfaces (also compare with Figure 6.2b).

The global transients are now simulated with SM. To reproduce the experiments, the probability distribution is propagated from a fully CO- or O-saturated surface. Figure 6.5 displays the corresponding calculations. Contrary to HeMF, the simulated transients qualitatively reproduce the experiments. Two stable steady states are present for Sample C, whereas the transients merge after a certain time for Sample A and Sample B. However, the fluctuation-induced transitions are considerably slower than observed experimentally.

Consequently, we use the rates from HeMF in SM. That is, the model now takes into account both fluctuations and sites with a weaker binding energy. As shown in Figure 6.5, a semi-quantitative agreement between the calculated and the experimental transients is obtained after adding a significant fraction of defect sites.

For HeMF, introduction of defect sites with a weaker CO adsorption shifts the steady states obtained from a CO- or O-precovered surface to lower Θ_{CO} and Θ_O, respectively. It thus reduces the distance between both steady states in coverage space (see Figure 6.2b). Therefore, spontaneous transitions between the two kinetic regimes are enhanced (compare Figure 6.4c and a with d and b, respectively). Although the system remains bistable, on a microscopic scale, as indicated by the existence of two probability maximums at high Θ_O and at high Θ_{CO}, the chance of finding the system in the transition regime is greatly increased, leading to a strongly shortened lifetime and thus to a fast dynamic equilibrium between both kinetic states.

6.6 Summary

We have shown for the case of CO oxidation on Pd surfaces that bistability and hysteresis effects, which are typical kinetic phenomena for several simple reactions on extended surfaces, vanish on particles in the nanometer size range. The evidence is derived from a systematic kinetic study employing molecular-beam techniques to different types of supported model catalyst systems, spanning a very broad range of particle sizes. By means of transient kinetic experiments and quantitative microkinetic simulations, it is demonstrated that the transition to the globally monostable kinetics is due to coverage fluctuations. These fluctuations occur in confined systems in the nanometer range and induce transitions between the two stable kinetic states. Defect sites, which are always present on a nanoparticle surface, are shown to play a crucial role on the timescale on which these transitions occur. In the specific case studied, the transition rate is found to be additionally enhanced in the small particle limit.